Control of dual three-phase IPMSM drive with cascaded DC-link capacitors for third generation EV

Control of dual three-phase IPMSM drive with cascaded DC-link capacitors for third generation EV

Andres Sierra-Gonzalez
TECNALIA, Basque Research and Technology Alliance (BRTA)
Bilbao, Spain
ORCID:0000-0002-7091-7485

Paolo Pescetto
Dep. of Energy Galileo Ferraris Politecnico di Torino
Torino, Italy
ORCID:0000-0002-9080-2749

Elena Trancho
TECNALIA, Basque Research and Technology Alliance (BRTA)
Bilbao, Spain
ORCID:0000-0002-2036-8115

Edorta Ibarra
Dep. of Electronics Technology Univ. of the Basque Country (UPV/EHU)
Bilbao, Spain
ORCID:0000-0002-2164-8573

Gianmario Pellegrino
Dep. of Energy Galileo Ferraris Politecnico di Torino
Torino, Italy
ORCID:0000-0003-4264-1917

Fernando Alvarez-Gonzalez
TECNALIA, Basque Research and Technology Alliance (BRTA)
Bilbao, Spain
ORCID:0000-0003-4854-1853

***Abstract*—In this work, a dual three-phase Interior Permanent Magnet Synchronous Machine (IPMSM) drive connected to a high voltage DC/DC converter (800 V) at its input is considered for electric vehicle (EV) applications. The drive is constituted by two cascaded three-phase inverters, enabling fast charging capabilities. In this particular configuration, balancing the input voltages of the two inverters is mandatory during operation. A novel control approach that not only provides such voltage balancing but also considers the cross-coupling effects of the dual-three phase IPMSM is proposed, guaranteeing an adequate torque regulation through the whole operation range of the drive. Simulation results, generated by means of a high fidelity platform, are provided to validate the proposed approach. Additionally, preliminary experimental results are also included.**

***Index Terms*—dual three-phase IPMSM, cascaded DC-link, multiphase, electric vehicles, voltage balancing, variable DC-link.**

I. Introduction

Multiphase electric drives are gaining attention over conventional three-phase solutions thanks to their merits, i.e., power splitting, high power density, high efficiency, lower torque pulsations and fault tolerance [1]–[3]. Among multiphase solutions, dual three-phase Permanent Magnet Synchronous Machines (PMSM) are being considered for electric vehicle (EV) applications, as the transition from manufacturing three-phase drives to dual three-phase ones is relatively straightforward [4], [5].

In general, the two three-phase sets of a dual three-phase PMSM are fed by two independent voltage source inverters (VSI), which DC-link capacitors are connected in parallel to an automotive battery pack (Fig. 1(a)). However, this research addresses the control of the drive proposed in [6], [7], which incorporates an intermediate high voltage DC/DC converter (Fig. 1(b)). This converter boosts the DC bus from the nominal battery voltage (400 V) to the 800 V range, allowing embedded compatibility with fast DC charging stations. Moreover, the DC-link voltage can be adapted in real time through a dedicated DC/DC control strategy. This way, it is possible to maximize the efficiency, allowing the optimal operation of the drive with independence of the state of charge (SoC) of the battery pack. However, inverters' input voltage is significantly increased. If the utilization of power semiconductors with high blocking voltages is to be avoided, a cascaded DC-link configuration can be considered (Fig. 1(b)), which allows to use semiconductors with half the blocking voltage.

In order to successfully control a dual three-phase IPMSM drive with such cascaded DC-link configuration, inverters' input voltages need to be balanced. This voltage balancing can be done by regulating the power circulating through each three-phase set of the drive. A straightforward control solution consists on using an independent three-phase Field Oriented Control (FOC) for each three-phase set. However, as demonstrated in [8], this approach does not consider the cross-coupling effects between winding sets, which has direct influence in the electromagnetic torque production of the machine. As a consequence, significant deviations from the commanded torque can be produced. For this reason, a decoupled FOC approach which makes use of convenient vector transformations and considers cross-coupling effects has been presented in [9], but authors did not address power splitting. Although this feature could be provided by regulating the fifth and seventh harmonics synchronous frame, this procedure is not straightforward.

Considering all the previous, this work proposes a novel decoupled dual three-phase IPMSM control strategy, referred to as *multiphase control approach*, that not only takes into consideration the cross-coupling effects of the machine but also incorporates input voltage balancing capabilities. This technique takes into account magnetic saturation and provides robust torque regulation under both Maximum Torque per Ampere (MTPA) and Field Weakening (FW) operation, making it suitable for Electric Vehicle (EV) applications.

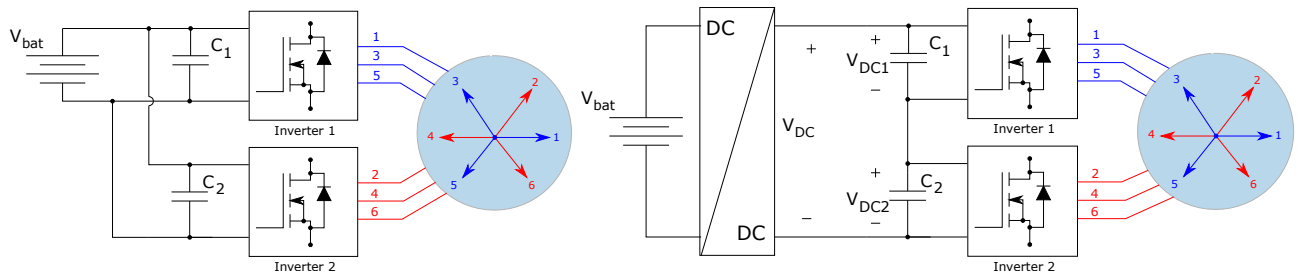

(a) (b)

Figure 1: General diagram of the dual three-phase IPMSM drive architecture for a winding displacement of $\alpha = \pi/3$: (a) conventional configuration, (b) cascaded DC-link capacitors with DC/DC converter.

The proposal is verified by simulations, and the obtained results are compared to the ones obtained by a proposed more conventional approach, consisting of two independent FOC controllers, referred to as *double three-phase control approach*. Finally, some preliminary experimental results showing the performance of the proposed *multiphase control approach* are also included.

II. Dual three-phase IPMSM mathematical model

For a 6-phase machine, (1) relates the phase voltages and currents in the natural (per-phase) reference frame.

$$\mathbf{V} = \mathbf{RI} + \frac{d\mathbf{LI}}{dt} + \frac{d\mathbf{\Psi}_{PM}}{dt}, \tag{1}$$

where $\mathbf{V} = [v_1, v_2, \ldots, v_6]$ and $\mathbf{I} = [i_1, i_2, \ldots, i_6]$ are the phase voltage and current vectors, $\mathbf{R} = R_s\mathfrak{I}$ is a 6×6 diagonal matrix that represents the phase resistances ($\mathfrak{I}$ is the identity matrix), and $\mathbf{L}$ is the 6×6 matrix which represents the self and mutual inductance of the machine. When the rotor has buried magnets, the elements of $\mathbf{L}$ vary according to the electrical angle of the rotor (θ_e). This effect is produced due to the variable magnetic reluctance of the IPMSM configuration [10]. Moreover, in automotive IPMSMs, $\mathbf{L}$ strongly varies with the stator current due to magnetic saturation. Finally, the vector $\mathbf{\Psi}_{PM} = [\Psi_1, \Psi_2, \ldots, \Psi_6]$ represent the per-phase magnetic flux linkages generated by the permanent magnets.

The electromagnetic torque generated by the motor is given by [11]:

$$T_{em} = \frac{1}{2}\mathbf{I}^T\frac{d\mathbf{L}}{d\theta_m}\mathbf{I} + \mathbf{I}^T\frac{d\mathbf{\Psi}_{PM}}{d\theta_m}, \tag{2}$$

where θ_m is the mechanical angular position.

Both (1) and (2) are sufficient for the mathematical representation of the electric machine. However, such model is complex and highly coupled, which makes it not appropriate for control system design. Therefore, vector transformations are applied to simplify the mathematical representation of the machine. These transformations allow the implementation of the well-known field-oriented control (FOC) technique.

Two vector transformations can be considered. The first is a generalization of the magnitude invariant Clarke-Park transform for symmetrical multiphase machines [9], [12], [13]. This transformation is called $\mathbf{T_1}$, it is illustrated in figure 2(a), and is given by:

$$\frac{1}{3}\begin{bmatrix} cos(\theta_e) & cos(\theta_e-\alpha) & \ldots & cos(\theta_e-5\alpha) \\ -sin(\theta_e) & -sin(\theta_e-\alpha) & \ldots & -sin(\theta_e-5\alpha) \\ cos(5\theta_e) & cos(5\theta_e-2\alpha) & \ldots & cos(5\theta_e-10\alpha) \\ -sin(5\theta_e) & -sin(5\theta_e-2\alpha) & \ldots & -sin(5\theta_e-10\alpha) \\ 1 & 0 & \ldots & 0 \\ 0 & 1 & \ldots & 1 \end{bmatrix}, \tag{3}$$

where, $\alpha = \pi/3$ is the spatial separation between adjacent phases.

The transformation matrix $\mathbf{T_1}$ allows to decouple and decompose the 6-dimension phase vectors (currents, voltages and fluxes) according to their harmonics components. If the homopolar components are not considered, $\mathbf{T_1}$ decomposes the phase variables into two decoupled subspaces. The two-dimensional reference frame D_1-Q_1 contain the fundamental components while the subspace D_2-Q_2 comprises the 5th and 7th harmonics.

The second transformation ($\mathbf{T_2}$) consists on the application of the conventional magnitude invariant three-phase Clarke-Park transformation to each three-phase set. This transformation is illustrated in figure 2(b), and is given by:

$$\begin{bmatrix} \mathbf{P_{3ph}}(\theta_\mathbf{e}) & \mathbf{0_{3\times3}} \\ \mathbf{0_{3\times3}} & \mathbf{P_{3ph}}(\theta_\mathbf{e} - \frac{\pi}{\mathbf{3}}) \end{bmatrix}, \tag{4}$$

where $\mathbf{P_{3ph}}(\theta_\mathbf{e})$ is the conventional three-phase Clarke-Park transformation.

$\mathbf{T_2}$ decomposes the 6-dimension phase vectors into two coupled subspaces. The plane d_1-q_1 contains the information related with the first three-phase set and the plane d_2-q_2 is related with variables (current, voltages and fluxes) of the second. Therefore, this transformation allows independent control of each three-phase current, but subject to cross-couplings.

The next step is to apply the transformations to (1) and (2). For $\mathbf{T_1}$ (figure 2(a)), we get the following vector model:

$$\begin{aligned} v_{D1} &= R_s i_{D1} + L_{D1}\frac{di_{D1}}{dt} - \omega_e L_{Q1} i_{Q1}, \\ v_{Q1} &= R_s i_{Q1} + L_{Q1}\frac{di_{Q1}}{dt} + \omega_e(L_{D1} i_{D1} + \psi_{PM1}), \end{aligned} \tag{5}$$

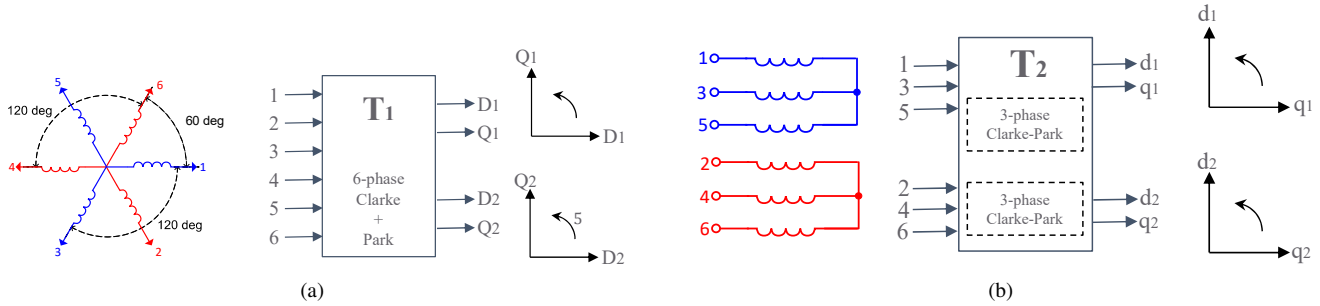

Figure 2: Vector transformations used in the proposed controller: (a) Multiphase approach (b) three-phase approach.

$$v_{D2} = R_s i_{D2} + L_{D2}\frac{di_{D2}}{dt} - 5\omega_e L_{Q2} i_{Q2}, \quad (6)$$
$$v_{Q2} = R_s i_{Q2} + L_{Q2}\frac{di_{Q2}}{dt} + 5\omega_e (L_{D2} i_{D2} + \psi_{PM5}),$$

$$T_{em} = 3N_p \left[\psi_{PM} i_{Q1} + (L_{D1} - L_{Q1}) i_{D1} i_{Q1}\right], \quad (7)$$

where N_p is the pole-pair number.

This vector model shows that both planes $D_1 - Q_1$ and $D_2 - Q_2$ are decoupled. These equations are quite similar to those of a three-phase IPMSM. The main difference is that the $D_2 - Q_2$ plane rotates at 5 times the angular speed of the $D_1 - Q_1$ plane. The parameters L_{D1}, L_{Q1}, ψ_{PM1}, L_{D2}, L_{Q2} and ψ_{PM5} are obtained by computing the per-phase finite element model (FEM) flux data.

Similarly, the result of applying the transformation $\mathbf{T_2}$ (figure 2(b)) over (1) and (2) results in:

$$v_{d1} = R_s i_{d1} + L_d\frac{di_{d1}}{dt} - \omega_e L_q i_{q1} + M_d\frac{di_{d2}}{dt} - \omega_e M_q i_{q2},$$
$$v_{q1} = R_s i_{q1} + L_q\frac{di_{q1}}{dt} + \omega_e L_d i_{d1} + \omega_e \psi_{PM} + M_q\frac{di_{q2}}{dt} - \omega_e M_d i_{d2}, \quad (8)$$

$$v_{d2} = R_s i_{d2} + L_d\frac{di_{d2}}{dt} - \omega_e L_q i_{q2} + M_d\frac{di_{d1}}{dt} - \omega_e M_q i_{q1},$$
$$v_{q2} = R_s i_{q2} + L_q\frac{di_{q2}}{dt} + \omega_e L_d i_{d2} + \omega_e \psi_{PM} + M_q\frac{di_{q1}}{dt} - \omega_e M_d i_{d1}, \quad (9)$$

$$T_{em} = \frac{3}{2}N_p[\psi_{PM}(i_{q1}+i_{q2}) + (L_d - L_q)(i_{d1}i_{q1} + i_{d2}i_{q2}) + (M_d - M_q)(i_{d1}i_{q2} + i_{d2}i_{q1})], \quad (10)$$

In this model, the planes $d_1 - q_1$ and $d_2 - q_2$ are coupled by the terms M_d and M_q. Therefore, the equations of voltages, currents, and torque are more complex than those of a three-phase motor. Another feature is that both planes rotate at the same speed, but there is a $pi/3$-radians offset between them. Both planes can produce torque, as shown by (10).

III. Torque Control for the Dual Three-Phase IPMSM with Cascaded DC-Link Capacitors

In this work, two torque control strategies for dual three-phase IPMSM with cascaded DC-link capacitors are proposed and compared considering the two vector model approaches described in the previous section. The first strategy, the *double three-phase torque control*, consists on the implementation of two independent torque control loops, one for each three-phase set. This strategy is based on the $\mathbf{T_2}$ transformation. The second strategy, the *multiphase torque control*, is based on both $\mathbf{T_1}$ and $\mathbf{T_2}$.

A. Double three-phase torque control

Figure 1(b) shows that the drive to be controlled has a non-conventional configuration. Due to the cascaded configuration of the 6-phase inverter, an active DC-link balancing strategy is required. The goal of this strategy is to evenly distribute the voltage at the output of the DC/DC converter. Therefore, the proposed controller is required to independently regulate the power consumed (or delivered during regenerative braking) by each three-phase set. In this way, if one of the input voltages of the inverter cells deviates from the desired value ($V_{DC}/2$), the control will be able to increase or decrease the power consumed by the respective three-phase set and correct the deviation.

A straightforward solution is to implement an independent torque control loop for each three-phase set. Therefore, well-known and validated control strategies for three-phase IPMSMs can be applied immediately. Considering this, a three-phase control solution, previously proposed by the authors in [14], has been adapted to the dual three-phase scenario. Figure 3 shows the related block diagram of the proposed controller created by following this approach, where each three-phase set is required to generate half of the desired torque.

In this solution, each three-phase set is treated as an independent machine. For each set, the torque controller can be divided into three stages. The first stage is responsible of generating the optimal current set-points considering the required torque and the actual state (currents, stator voltage and speed) of the machine. The second stage incorporates the active voltage balancing functionality. Finally, the third stage includes the synchronous current regulation loops.

For the generation of optimal current set-points, a simple solution with a relatively low computational burden consists on precalculating these references, storing them into Look-up tables (LUTs). In general, 3D-LUTs are required for automotive IPMSMs, as the optimal current set-points are dependent on

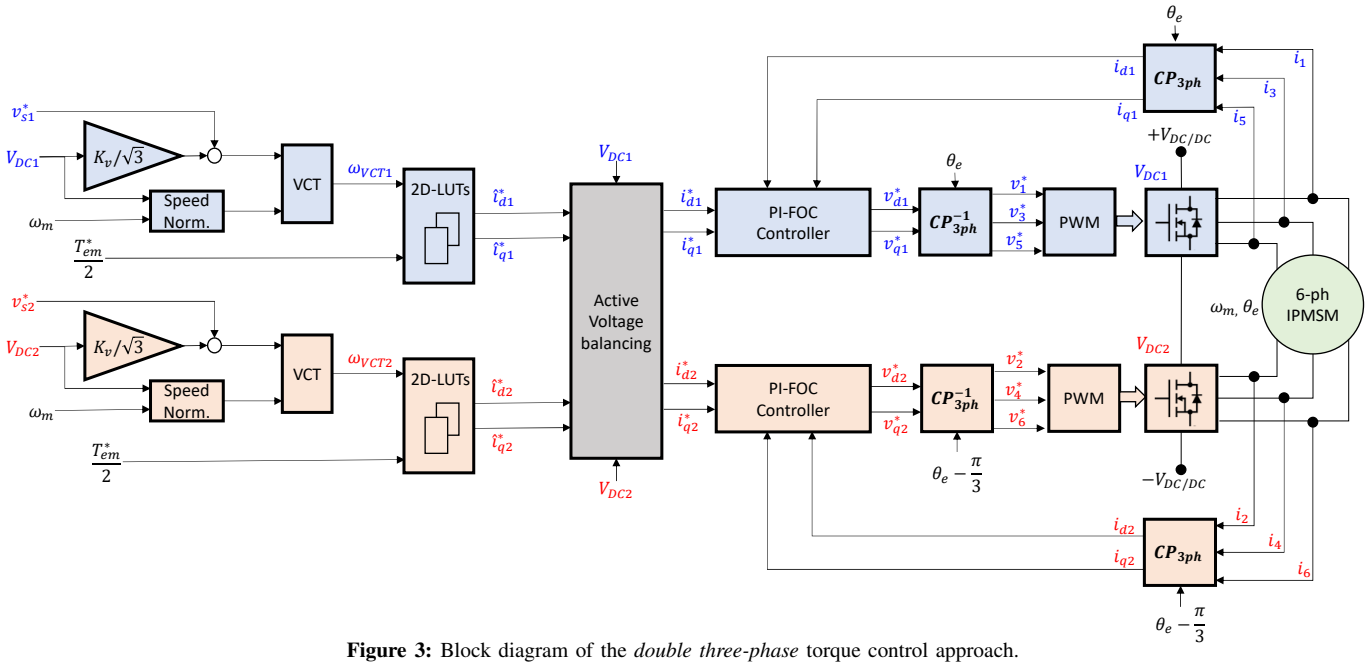

Figure 3: Block diagram of the *double three-phase* torque control approach.

the reference torque, DC-link voltage and mechanical speed. Usually, rotor temperature is not considered in industrial applications as its precise estimation is complex. The LUTs are calculated for a specific set of electrical parameters, and control can be eventually lost in field weakening if significant parameter variations due to machine ageing or manufacturing tolerances occur [14].

In the implemented strategy, LUTs dimensions are reduced to only two (speed and torque), as speed can be normalized. Besides, to address the parameter variations issues, a Voltage Constraint Tracking (VCT) feedback is used [14]. Figure 4 shows the VCT structure. The goal of the VCT is to maintain the stator voltage vector close to the voltage limit margin during field weakening operation. To achieve this, the VCT varies the mechanical speed fed to the 2D-LUTs according to the error produced between the current control reference voltage v_s^* and the voltage limit ($V_{DC}/\sqrt{3}$).

For the implementation of the VCT, the constants k_v and k_{vct} needs to be defined. k_v is selected from $0.8 < k_v < 1$ to ensure that the voltage limit is never reached. The constant $k_{vct} > 0$ is tuned to adjust the dynamics of the VCT regulator properly. Therefore, this strategy does not require to know any machine parameters, providing additional robustness to the well-known LUT based set-point generation technique under parameter variations or uncertainties.

Then, the resulting current references are modified to balance the DC voltage of each three-phase cell. Figure 5 shows the block diagram of the algorithm proposed to ensure the DC-link voltage balancing. As shown in the figure, this block modifies the current references according to the error between the measured DC-link voltage of each cell and the desired reference ($V_{DC}/2$). For simplicity, it has been chosen to modify only the current set-points i_{q1}^* and i_{q2}^*. In the constant

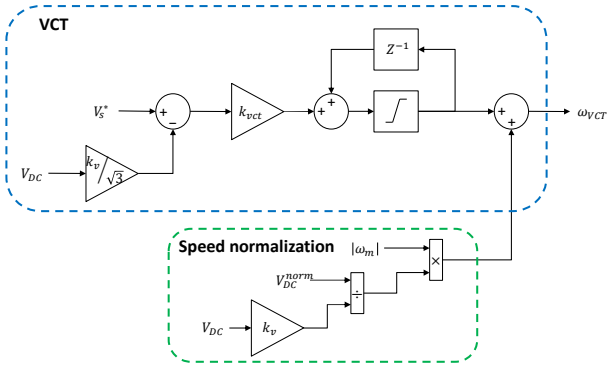

Figure 4: Block diagram of the VCT feedback loop.

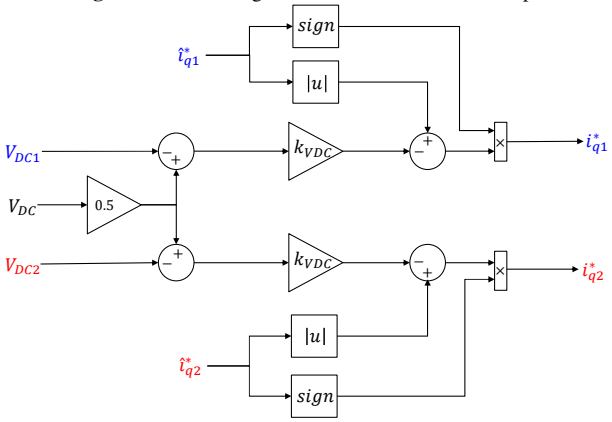

Figure 5: Block diagram of the proposed active voltage balancing algorithm.

torque region, this causes a small deviation from the MTPA locus. However, the discrepancy is lower than 5 % and is considered acceptable.

The last stage of the double three-phase torque controller consists of two conventional current control loops, one for each three phase set [15]. These current control loops include

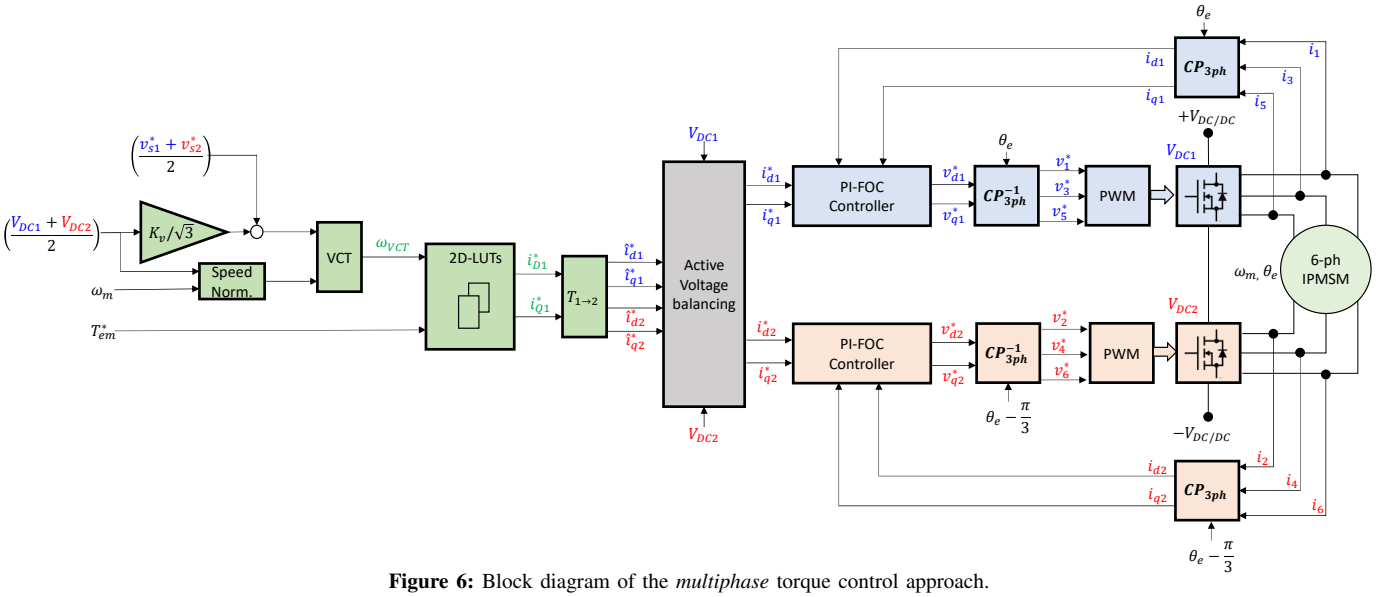

Figure 6: Block diagram of the *multiphase* torque control approach.

Proportional-Integral controllers (PI), decoupling feed-forward terms and anti-windup schemes. Then, the voltage references are transformed from $d-q$ to the respective three-phase values. Finally, PWM blocks synthesize the firing pulses for each inverter cell.

The *double three-phase torque control* has two main advantages. The first one is the straightforward application of well-known control techniques used for decades for the control of three-phase machines. The second one is the independent power control of each three-phase set, required for DC voltage balancing. However, this approach does not address the coupling between sets. Therefore, deviations are expected from the optimum operation points. In order to avoid this disadvantage, a new control strategy, which is described bellow, is proposed.

B. Multiphase torque control

Figure 6 shows the block diagram of the proposed *multiphase torque control* strategy. The aim of this approach is to keep the advantages of the *double three-phase torque control* while avoiding its drawbacks. Therefore, the independent current control loops and the active DC voltage balancing stages remain unchanged. However, the generation of optimal current set-points is updated to consider coupling between three-phase sets.

The structure of the currents set-points generation algorithm is quite similar to the previous one. However, in this case the current generation is done in the $D-Q$ frames. Therefore, the motor is considered as a unit, where both sets interact to produce the required torque. For the calculation of the required 2-D LUTs, the model represented by (5), (6) and (7) has to be considered. Then, the optimum currents LUTs are calculated from phases flux data computed from the IPMSM FEM model. As the currents $i_{D1}-i_{Q1}$ are the responsible for producing torque, only two LUTs are required.

As in the previous approach, the VCT scheme of figure 4 is implemented to provide additional robustness against parameter uncertainties. However, in this case the average of the reference stator voltages (v_{s1}, v_{s2}) and DC-link input voltages (V_{DC1}, V_{DC2}) are considered to feed the VCT loop. Other difference of the *multiphase torque control* over the *double three-phase torque control* is that the LUTs are fed with the full required torque instead of half torque.

Once the optimal set-points $i^*_{D1}-i^*_{Q1}$ are calculated, they are transformed into the d_1-q_1 and d_2-q_2 planes. This is done thanks to the transformation $T_{1\to2}$:

$$\begin{bmatrix} d_1 \\ q_1 \\ h_1 \\ d_2 \\ q_2 \\ h_2 \end{bmatrix} = \begin{bmatrix} 1 & 0 & cos(6\theta_e) & -sin(4\theta_e) & 0 & 0 \\ 0 & 1 & -sin(6\theta_e) & cos(4\theta_e) & 0 & 0 \\ 0 & 0 & 0 & 0 & 1 & 0 \\ 1 & 0 & -cos(6\theta_e) & sin(6\theta_e) & 0 & 0 \\ 0 & 1 & sin(6\theta_e) & cos(6\theta_e) & 0 & 0 \\ 0 & 0 & 0 & 0 & 0 & 1 \end{bmatrix} \begin{bmatrix} D_1 \\ Q_1 \\ D_2 \\ Q_2 \\ H_1 \\ H_2 \end{bmatrix}. \tag{11}$$

The rest of the control blocks are equal for both proposed techniques.

IV. Validation of the Proposed Torque Controller

A. Simulation results

In order to validate the proposal, the dual three-phase IPMSM drive presented in [6], [7] has been considered, which most relevant parameters are shown in table I. An accurate model of the electric drive has been simulated in Matlab/Simulink. The model includes the cross-coupling and magnetic saturation effects of the dual three-phase machine.

Figure 7 shows the performance of the drive when the *double three-phase control approach* is used for torque regulation. In this test, the machine is operated over the whole speed range while a torque of reference of 80 Nm is commanded and the maximum power limit of 135 kW is imposed. The DC-link voltage balance is ensured during the test. As expected, a small deviation on torque is observed during MTPA operation. During FW, the torque deviation increases with the speed. Furthermore, a non-smooth stator voltage tracking is noted.

Table I: Most relevant nominal parameters of the automotive dual three-phase IPMSM drive.

Parameter	Value
Pole-pair number (N_P)	3
Nominal power (P_{nom})	70 kW
Maximum power (P_{max})	135 kW
Maximum mechanical speed ($w_{mech,max}$)	22000 rpm
Maximum torque ($T_{em,max}$)	170 Nm
Maximum current per winding (I_{max})	235 Arms
Switching frequency (f_{sw})	12 kHz
DC/DC converter output voltage	450 V to 750 V
Battery voltage	320 V to 400 V

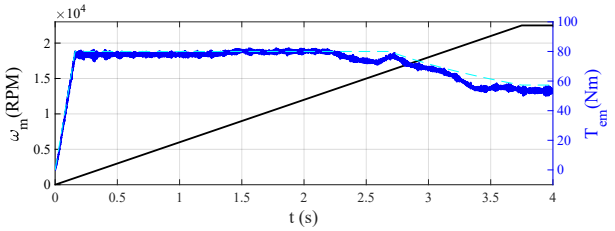

(a) Torque and speed.

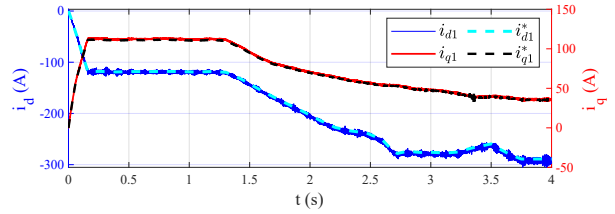

(b) Synchronous reference frame currents.

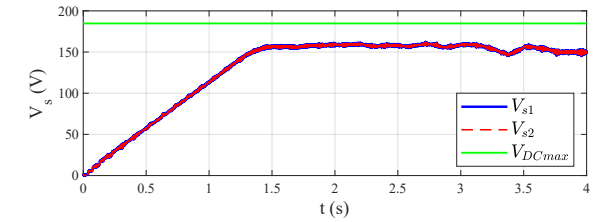

(c) Field weakening control results.

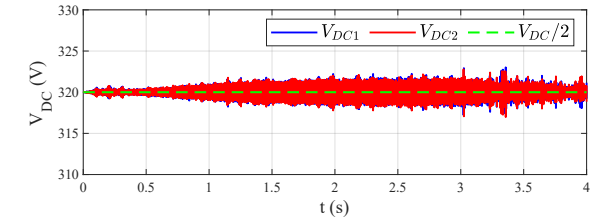

(d) Voltage balancing control results.

Figure 7: Dual three-phase IPMSM regulation using the *double three-phase control approach*.

All these phenomena occur because the coupling between the two three-phase sets has been neglected.

On the other hand, figure 8 shows the drive performance for same operating conditions when the *multiphase control approach* is used for torque regulation. As the proposed controller considers the coupling effects of the machine, no deviations between the commanded and the obtained torque are produced during MTPA. The field weakening operation is correctly performed considering a security margin of 10 % of maximum stator voltage ($k_v = 0.9$). Note that, in this particular test and as a result of the quantization of the LUT data, the VCT algorithm is activated at around $t = 3.5$ s, maintaining the voltage constraint limit during the transition between FW and Maximum Torque per Voltage (MTPV) regions (this transition can be smoothed by increasing the amount of data stored in the LUTs). Again, the voltage balancing is satisfactorily performed for all the operation regions (figure 8(d)).

Figure 9 shows analogous results when a stretch of a World Harmonized Light-duty Vehicle Test Procedure (WLTP) driving cycle is applied over the dual three-phase drive and the *multiphase control approach* is used. Hereafter, figure 10 illustrates why the current balancing algorithm is mandatory, as DC-link voltages become highly unbalanced when this control block is deactivated, leading to a loss of control.

Finally, figure 11 shows operation when the optimal DC voltage adaptation strategy, proposed in [16], is integrated into the drive control system. This online strategy varies the DC-link voltage depending the speed and torque operating points in order to minimize the power losses in the DC/DC converter and inverter.

B. Preliminary experimental results

Finally, a preliminary set of low power tests has been carried out to experimentally validate the *multiphase torque control*. The prototype of figure 12 has been used, which most relevant nominal parameters are, once again, the ones summarized in table I.

As an example, figure 13 shows the results obtained for a particular set of low speed and low torque operation conditions, where various torque steps are commanded and the expected control results are obtained both regarding torque regulation and DC-link voltage balancing.

V. Conclusion

This work proposes two novel control structures, for torque control of multiphase machines under cascaded connected DC-link inverters, able to guarantee the correct balancing of the two DC-link voltages. The approach *multiphase torque control* considers the inherent cross-coupling between the two 3-phase sets and demonstrated to be superior respect to the more conventional *double three-phase control* approach.

To take full advantage of the hardware configuration and the capabilities of the proposed control, as future work, an optimal DC-link voltage adaptation strategy will be integrated into the experimental drive control system. In addition, further experimental validation of the control system will be carried out under nominal operation conditions.

Acknowledgment

This research has received funding from the European Union's Horizon 2020 research and innovation programme

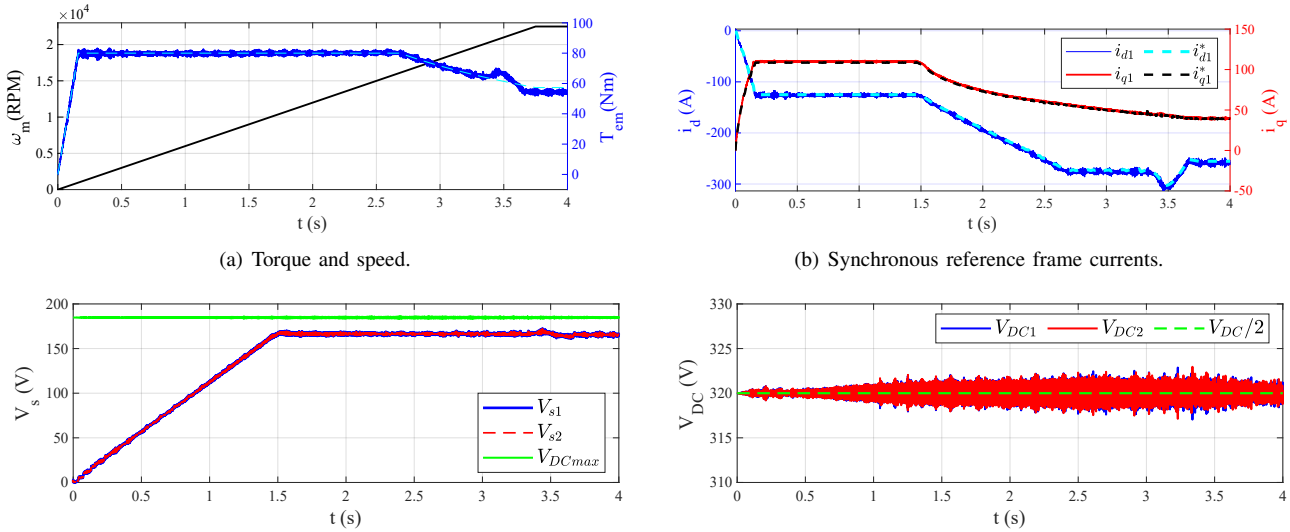

(a) Torque and speed.

(b) Synchronous reference frame currents.

(c) Field weakening control results.

(d) Voltage balancing control results.

Figure 8: Dual three-phase IPMSM regulation using the *multiphase control approach* (I): nominal torque operation over the whole speed range.

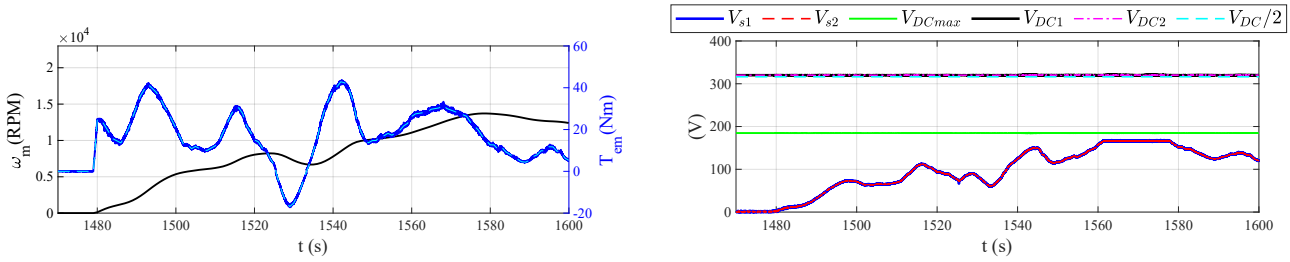

(a) Torque and speed.

(b) DC-link and stator voltage control results.

Figure 9: Dual three-phase IPMSM regulation using the *multiphase control approach* (II): WLTP driving cycle test results.

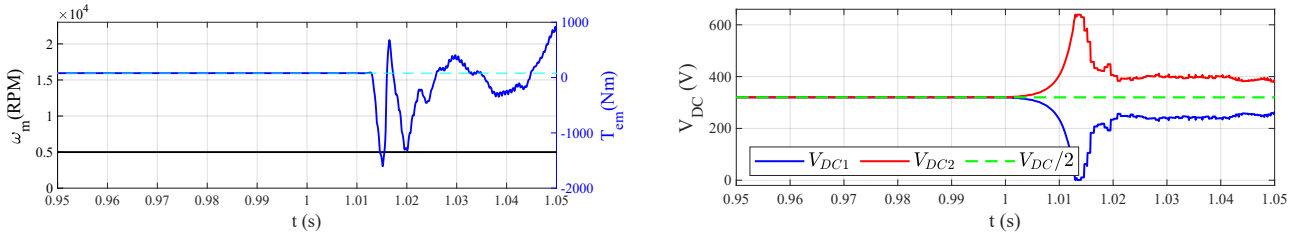

(a) Torque and speed.

(b) Voltage balancing control results.

Figure 10: Dual three-phase IPMSM regulation using the *multiphase control approach* (III): disconnection of the voltage balancing control at $t = 1$ s.

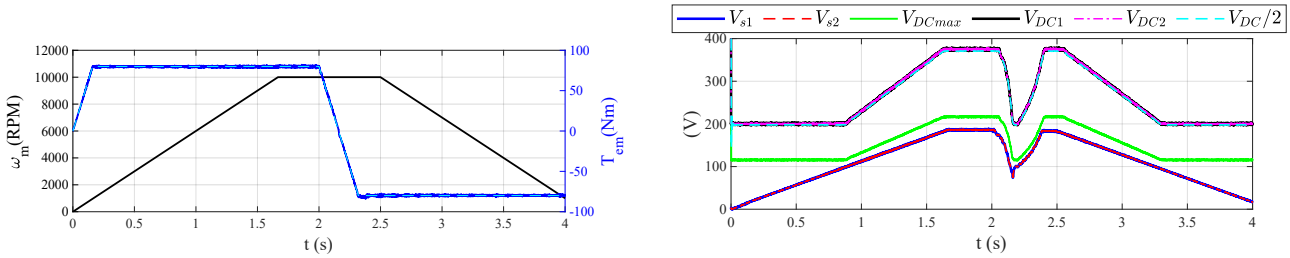

(a) Torque and speed.

(b) Voltage balancing control results.

Figure 11: Dual three-phase IPMSM regulation using the *multiphase control approach* (IV): optimal DC voltage adaptation

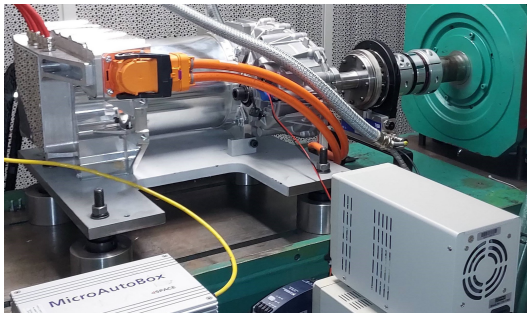

Figure 12: Experimental platform including the dual three-phase IPMSM (provided by BRUSA Elektronik AG).

under project FITGEN grant agreement No 824435. This work has been supported in part by the Government of the Basque Country within the fund for research groups of the Basque University system IT978-16 and the research program ELKARTEK (project ENSOL2-KK-2020/00077), and also by the Ministerio de Ciencia e Innovación of Spain within the project PID2020-115126RB-I00 and FEDER funds.

REFERENCES

[1] F. Barrero and J. Duran, "Recent advances in the design, modelling and control of multiphase machines," *IEEE Transactions on Industrial Electronics*, vol. 63, no. 1, pp. 449–458, 2016.

[2] G. Feng, C. Lai, W. Li, Y. Han, and N. Kar, "Computation-efficient solution to open-phase fault tolerant control of dual three-phase interior PMSMs with maximized torque and minimized ripple," *IEEE Transactions on Power Electronics*, vol. 36, no. 4, pp. 4488–4499, 2021.

[3] Cui, "Improved DC-link voltage utilization for dual three-phase drives with full anti-windup and harmonic compensation," in *Proc. of the IEEE International Conference on Industrial Technology (ICIT)*, 2021, pp. 203–208.

[4] A. Salem and M. Narimani, "A review on multiphase drives for automotive traction applications," *IEEE Transactions on Transportation Electrification*, vol. 5, no. 4, pp. 1329–1348, 2019.

[5] A. Matallana, E. Ibarra, I. López, J. Andreu, J. Garate, X. Jorda, and J. Rebollo, "Power module electronics in HEV/EV applications: New trends in widebandgap semiconductor technologies," *Renewable and Sustainable Energy Reviews*, vol. 113(109264), pp. 1–33, 2019.

[6] M. De Gennaro, P. Scheuermann, T. Wellerdieck, V. Ravello, G. Pellegrino, and E. Trancho, "The H2020 project FITGEN: preliminary results and design guidelines of an integrated e-axle for the third-generation electric vehicles," in *Proc. of the 8th Transport Research Arena (TRA)*, 2020, pp. 1–10.

[7] M. Martino, P. Pescetto, and G. Pellegrino, "Advanced functionally integrated E-Axle for A-Segment electric vehicles," in *2020 AEIT International Conference of Electrical and Electronic Technologies for Automotive*, 2020, pp. 1–6.

[8] J. Karttunen, S. Kallio, P. Peltoniemi, P. Silventoinen, and O. Pyrhonen, "Dual three-phase permanent magnet synchronous machine supplied by two independent voltage source inverters," in *Proc. of the International Symposium on Power Electronics Power Electronics, Electrical Drives, Automation and Motion (SPEEDAM)*, 2012.

[9] J. Karttunen, S. Kallio, P. Peltoniemi, P. Silventoinen, and O. Phyronen, "Decoupled vector control scheme for dual three-phase permanent magnet synchronous machines," *IEEE Transactions on Industrial Electronics*, vol. 61, no. 5, pp. 2185–2196, 2014.

[10] M. A. Rahman, *Power Electronics and Motor Drives*. CRC Press, 2016, ch. Permanent Magnet Machines, pp. 5–1, 5–10.

[11] A. Sierra-González, E. Ibarra, I. Kortabarria, E. Trancho, and E. Otaola., "Real-time simulation platform of an EMA landing gear," in *Proc. of the 11th IET International Conference on Power Electronics, Machines and Drives (PEMD 2020)*, 2020, pp. 1–6.

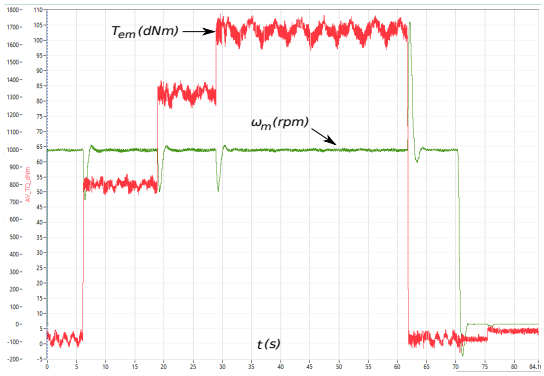

(a) Torque and mechanical speed.

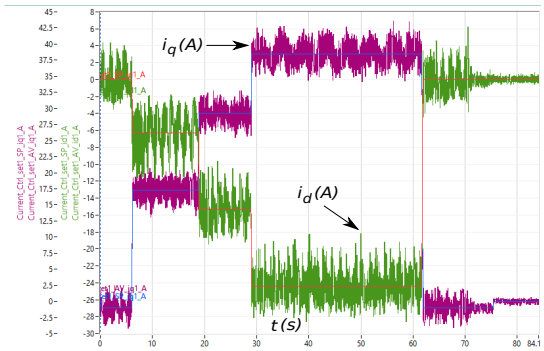

(b) d- and q-axis currents.

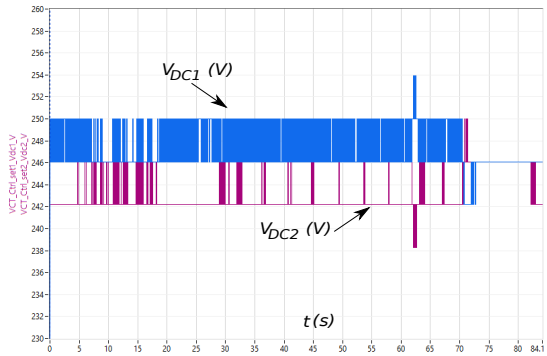

(c) DC-link voltage regulation.

Figure 13: Preliminary experimental results obtained from CAN data.

[12] S. Kallio, M. Andriollo, A. Tortella, and J. Karttunen, "Decoupled $d-q$ model of double-star interior-permanent-magnet synchronous machines," *IEEE Transactions on Industrial Electronics*, vol. 60, no. 6, pp. 2486–2494, 2013.

[13] M. Benkhoris, *Control of the Double-star Synchronous Machine Supplied by PWM Inverters*. John Wiley & Sons, Ltd, 2012, ch. 4, pp. 125–159.

[14] E. Trancho, E. Ibarra, A. Arias, I. Kortabarria, J. Jurgens, L. Marengo, and A. Fricasse, "PM-assisted synchronous reluctance machine flux weakening control for EV and HEV applications," *IEEE Transactions on Industrial Electronics*, vol. 65, no. 4, pp. 2986–2995, 2018.

[15] Y. Hu, Z. Q. Zhu, and M. Odavic, "Comparison of two-individual current control and vector space decomposition control for dual three-phase PMSM," *IEEE Transactions on Industry Applications*, vol. 53, no. 5, pp. 4483–4492, 2017.

[16] P. Pescetto, A. Sierra-Gonzalez, E. Trancho, and G. Pellegrino, "Variable dc-link control strategy for maximum efficiency of traction motor drives," in *Proc. of the 2021 IEEE Energy Conversion Congress and Exposition (ECCE)*, 2021, pp. 1–8.